remote sensing

MDPI

Communication

Characteristics and Mechanisms of Marine Heatwaves in the East Asian Marginal Seas: Regional and Seasonal Differences

Wonkeun Choi [1,2], Minkyoung Bang [1,3], Youngji Joh [4], Yoo-Geun Ham [5], Namyoung Kang [6] and Chan Joo Jang [1,2,3,*]

1 Ocean Circulation Research Center, Korea Institute of Ocean Science and Technology, Busan 49111, Korea; dnjsrms@kiost.ac.kr (W.C.); b910111@kiost.ac.kr (M.B.)
2 Department of Ocean Science, University of Science and Technology, Daejeon 34113, Korea
3 Ocean Science and Technology School, Korea Maritime and Ocean University, Busan 49112, Korea
4 Atmospheric and Oceanic Sciences Program, Princeton University, Princeton, NJ 08544, USA; youngji.joh@princeton.edu
5 Department of Oceanography, Chonnam National University, Gwangju 61186, Korea; ygham@jnu.ac.kr
6 Department of Geography, Kyungpook National University, Daegu 41566, Korea; nkang4@knu.ac.kr
* Correspondence: cjjang@kiost.ac.kr

Abstract: Characteristics of marine heatwaves (MHWs) in the East Asian Marginal Seas (EAMS) were investigated using the daily Optimum Interpolation Sea Surface Temperature for 37 years (1982–2018), focusing on seasonal changes and regional differences. The summer MHWs occur 54% more frequently (2.7 events/decade) in a relatively wide area than in other seasons. The strong (up to 3.7 °C) and long-lasting (up to 38 days/event) winter MHWs are concentrated along the subpolar front (SPF) in the East/Japan Sea (EJS) where the MHWs are 20% longer (2.2 days/event) than in the Yellow and East China Seas (YECS). The summer MHWs are primarily driven by increased shortwave radiation associated with reduced cloud cover and latent cooling from the weakened wind over the western flank of developing subtropical highs. Driving mechanisms of the winter MHWs differ by region. The YECS MHWs occur mainly due to the atmospheric processes associated with weakening continental highs, while the EJS MHWs are largely driven by the northward shift of the SPF. Although large-scale atmospheric processes primarily drive the summer MHWs occurring in a wide area in the EAMS, our findings suggest that ocean processes can be major contributors to intensified MHW generation in limited areas, especially in winter.

Keywords: marine heatwaves; sea surface temperature; ocean dynamics; atmospheric forcing; composite analysis; extreme climate

Citation: Choi, W.; Bang, M.; Joh, Y.; Ham, Y.-G.; Kang, N.; Jang, C.J. Characteristics and Mechanisms of Marine Heatwaves in the East Asian Marginal Seas: Regional and Seasonal Differences. *Remote Sens.* **2022**, *14*, 3522. https://doi.org/10.3390/rs14153522

Academic Editor: Sergei Badulin

Received: 2 June 2022
Accepted: 18 July 2022
Published: 22 July 2022

1. Introduction

Marine heatwaves (MHWs), which are extreme climate events wherein the ocean temperature substantially increases over thousands of kilometers for periods ranging from a few days to years, are increasing in frequency and intensity with global warming [1–7]. MHWs have been observed previously around the world [8–12]. Along Western Australia during 2010–2011, MHWs were induced by air–sea interactions, such as an intensified Leeuwin Current, a strong La Niña, and increased heat flux from the atmosphere [8]. From 1993 to 2015, MHWs in eastern Australia were mainly caused by the strengthening of the East Australian current [12]. In 2014–2015, MHWs in the Northeast Pacific triggered by the North Pacific Gyre Oscillation induced the tropical El Niño–Southern Oscillation (ENSO) and increased the frequency of Northeast Pacific MHWs by strengthening the Pacific Decadal Oscillation (PDO) in the following winter [10,13]. MHWs impact the overall marine ecosystem across trophic levels through changes in habitat distribution, biodiversity, and communities [14]. In the global ocean, during MHW events, phytoplankton blooms were weakened in nutrient-poor waters, whereas they strengthened in nutrient-rich waters [15].

In Korean waters, summer MHWs contribute to the slow growth and advanced timing of dinoflagellate blooms through strong stratification [16]. The effects of these MHWs on primary production can also cascade up to the upper trophic level. In the northwestern Mediterranean in summer of 2003, MHWs induced mass mortality events comprising more than 25 benthic invertebrate species [17]. On the west coast of Australia in 2011, MHWs triggered benthic habitat migration and widespread death of cold-water species [18–21]. In the Northwest Atlantic in 2012, MHWs affected changes in the distribution of the longfin squid [22].

MHWs can have different impacts on marine ecosystems in different seasons. Survival, growth, reproduction, and species interactions respond differently each season to changes in the solar radiation, day length, and temperature [23]. MHWs can interrupt seasonal growth and may induce relatively warm temperatures above the species-specific thresholds during different seasons [24]. For example, several seaweed species reproduce in winter, during which the early life stages are more susceptible to heat stress than the adult stage [25,26]. Considering that the MHW impact on the marine ecosystem varies according to season, understanding the seasonal differences in MHW characteristics is a key issue.

As MHWs have recently attracted scientific and societal interest, various underlying mechanisms have been investigated [9–13]. The East Asian Marginal Seas (EAMS; the East/Japan Sea, the Yellow Sea, the East China Sea, and the Bohai Sea) experience a high frequency of MHWs compared with the rest of the world [9]. In China's marginal seas, including the Yellow, East China, and Bohai Seas (YECS), the duration, frequency, and mean intensity of MHWs are more than twice the global average [27]. In the EAMS, MHWs are also driven by various mechanisms of atmospheric forcing and ocean dynamics. Two major modes of East Asian summer MHWs from 1982 to 2018 were revealed to be related to two contrasting sea surface temperature (SST) patterns over the subtropical western North Pacific [11]. MHWs in China's marginal seas and offshore waters can be generated by increased solar radiation owing to reduced cloud cover, weak wind speeds that diminish ocean heat loss, a weak and warm Kuroshio Current, and strong El Niño events [27]. MHW characteristics in the East/Japan Sea (EJS) from 1982 to 2020 show that in summer and fall, the MHWs were spatially distributed more homogeneously, whereas in spring and winter, the MHWs occurred concentrated in the west and center of the EJS [9].

The seasonal difference in EJS MHW distribution, which is wide in summer and local in winter, suggests the possibility of MHWs occurring mainly due to atmospheric forcing in summer but primarily due to ocean dynamics in winter. However, ocean and atmospheric dynamics, which can drive MHWs, differ across seasons and regions. For example, in the EJS, the expansion and contraction of the North Pacific high pressure in summer induce changes in warm air flow over the EJS from the subtropics/tropics [28], and changes in winter wind speed influence the sensible heat flux through entrainment of the cold water beneath the mixed layer, resulting in SST changes [29]. In the Yellow and East China Seas, stratification, due to the barrier effect of the Yangtze River (or Changjiang), is discharged in summer [30], and a strengthened (weakened) wind field owing to negative (positive) Arctic Oscillation (AO) in winter affects changes in the SST [31]. Therefore, the characteristics and mechanisms of MHWs possibly differ across seasons and regions. In this study, we aimed to examine the characteristics and the mechanisms of both seasonal and regional MHWs, focusing on air–sea interactions.

This paper is organized as follows. Section 2 describes the data and methods used in this study; the characteristics and mechanisms of MHWs in different seasons and regions in the EAMS are described in Section 3; finally, Section 4 provides a discussion and concluding remarks regarding the major findings.

2. Data and Methods

2.1. Data Description

Thirty-seven years of data (1982–2018) from the National Oceanic and Atmospheric Administration and the Optimum Interpolation SST version 2 (OISST v2) were used for

this study [32]. The OISST has a horizontal resolution of 0.25° and a daily time scale. The research area included the EAMS bounded by 115.5–142.5°E, 24–52°N (Figure 1). To compare the characteristics and mechanisms of MHWs according to the region, the research area was divided into two regions: the EJS (128–142.5°E, 34–52°N) and the Yellow and East China Seas, including the Bohai Sea (YECS; the rest of the research area excluding the EJS). Information on the land–sea boundaries was provided by the National Institute of Fisheries Science.

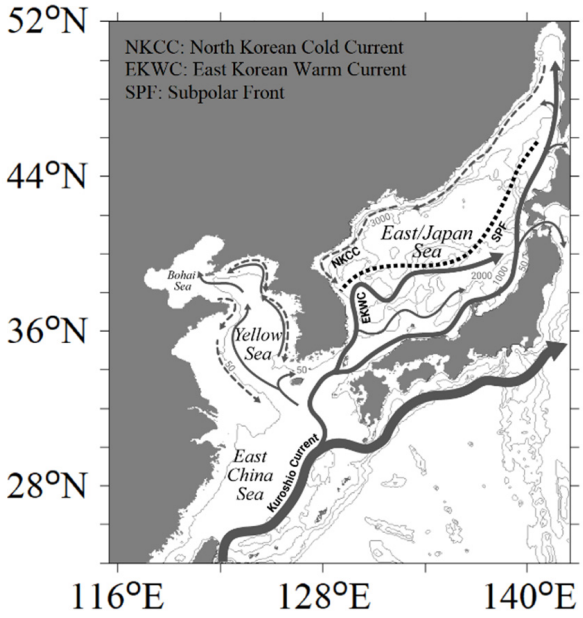

Figure 1. Schematic map of the surface currents overlaid on the bottom topography in East Asian Marginal Seas separated into two regions: the East/Japan Sea (EJS) and the Yellow & East China Seas, including the Bohai Sea (YECS). Solid (dashed) arrows indicate the warm (cold) ocean current. The dotted line indicates the subpolar front (SPF).

To detect the influence of the atmosphere on the occurrence of MHWs, 6-hourly fifth generation European Centre for Medium-Range Weather Forecasts reanalysis data (ERA5) were used [33]. To make the time interval of ERA5 the same as that of the OISST, we calculated the daily average using 6 h interval data and matched the spatial grid equally through bilinear interpolation. The parameters used herein included total cloud cover, 10 m winds, 500 hPa geopotential height, surface net solar radiation, and surface latent heat flux. The wind stress curl was calculated using the 10 m wind data.

To examine the influence of the ocean dynamics on the MHW mechanisms, surface ocean current data derived from satellite altimeter data provided by the Korea Hydrographic and Oceanographic Agency (KHOA) were used [34]. The data period was 26 years, from 1993 to 2018, which is shorter than the OISST, with equal daily intervals. The horizontal resolution is 0.25°, and the spatial coverage is 127–142°E, 34–48°N, slightly narrower than the EJS area. For seasonal analysis, all data were divided into four seasons, considering the thermal inertia of the ocean due to the large ocean heat capacity as follows: spring (April–June), summer (July–September), fall (October–December), and winter (January–March).

2.2. Definition of MHWs

MHWs were detected from daily SST time series using the definition of Hobday et al. (2016) [35]: (1) This method calculates the climatology and threshold using the mean and the 90th percentile of daily SST within an 11-day moving window across the baseline period (1982–2011). For example, on 15 June, the climatology and threshold are calculated using the mean and 90th percentile of all SST from 10 June to 20 June, a total of

330 samples during the baseline period. (2) Applying a 31-day moving average to smooth the climatology and threshold. (3) The SST exceeding the threshold by more than 5 days is defined as an MHW. If two MHWs are separated by fewer than 2 days, they are considered the same MHW. In the study, a 30-year period was configured as climatology in order to interpret the results as anomalies, which is conceptually different from examining the annual deviation from the climatology over the entire period, i.e., 37 years. The prior portion of the entire period, i.e., 1982–2011, was chosen for the climatological baseline. The MHW intensity is defined as an SST anomaly from the climatological baseline during the MHW period, representing how anomalously warm the MHW is compared to the climatology. The MHW analysis was performed in R language, using the package "heatwaveR" version 0.4.5 [36], based on the MHW definition by Hobday et al. (2016).

MHWs that persisted and exceeded 3 months/one season were classified into the beginning season of the MHW. For example, if an MHW started on 10 March and ended on 20 July, this MHW was classified as a winter (March) MHW because the mechanism in winter (March) induced this MHW.

This study investigated three MHW characteristics: total days (i.e., the sum of MHW days per year), frequency (i.e., the number of MHWs that occurred in a year), and mean intensity (i.e., the average intensity of MHWs over the entire period). Instead of duration, the total number of days was mainly used to indicate how long MHWs persist after their occurrence. "Total days" represents the sum of the MHW occurrence periods, whereas "duration" is the average of each MHW occurrence period; the duration is reduced when MHWs frequently occur within a relatively short period. Therefore, "total days" better reflects the impact of MHWs on the marine ecosystem because it considers the long-lasting and frequent impacts of MHW.

2.3. Criteria of Composite Analysis

To analyze the mechanisms of MHW generation, a composite analysis of atmospheric and ocean variables was used. Based on the spatial coverage, duration, and mean intensity of MHWs, composite periods were selected when values for all criteria were in the top third (strong MHW period) and bottom third (weak MHW period). The atmospheric and oceanic variables were then averaged for the MHW duration corresponding to each selected period. When other criteria, such as the top and bottom quarter, were used, the main drivers in each season or region remained the same with a negligible difference in the composite patterns; thus, in this study, the top and bottom third, which showed more considerable changes, were used. The reason for comparing the bottom third instead of non-occurrence MHW days is that MHWs occur in more than one grid almost every day in the EAMS. In summer, the bottom third of spatial coverage is only 8 grids (0.22%). Therefore, if MHWs occur within the bottom third of spatial coverage, mean intensity, and duration, they can be considered negligible.

In KHOA surface ocean current data, for the criteria of composite analysis, all daily data for months in which strong MHWs occurred were used instead of data from selected days because the number of data points was insufficient owing to the short data period.

The significance of the composite difference was measured using a Student *t*-test between the strong and weak MHW periods for each grid.

3. Results

3.1. MHW Characteristics

MHW characteristics were classified into three categories, namely, the total days, frequency, and mean intensity. The spatial mean of total MHW days was 26.7 days/year, ranging from 17.5 to 40.2 days/year during the 37 years in EAMS (Figure 2a). Regionally, in the EJS, the spatial mean of total days was 27.5 days/year, and that in the YECS was 26.1 days/year. The higher-value regions, defined as the 99th percentile of all grids (35.2 days/year), were located on the east coast of the Korean peninsula, Tsugaru Strait, the coast of the Bohai Sea, and the southern part of the East China Sea. In contrast, MHWs

shorter than 19.3 days/year (1st percentile of all grids) were located near the Korea Strait (approximately 128°E, 34°N). The frequency of MHWs ranged from 1.49 to 3.27 events/year during the 37 years in the EAMS, and the spatial mean was 2.18 events/year in the EJS and 2.35 events/year in the YECS. The higher-value region where MHWs occurred more than 3 times per year was located in the Kuroshio region (Figure 2b).

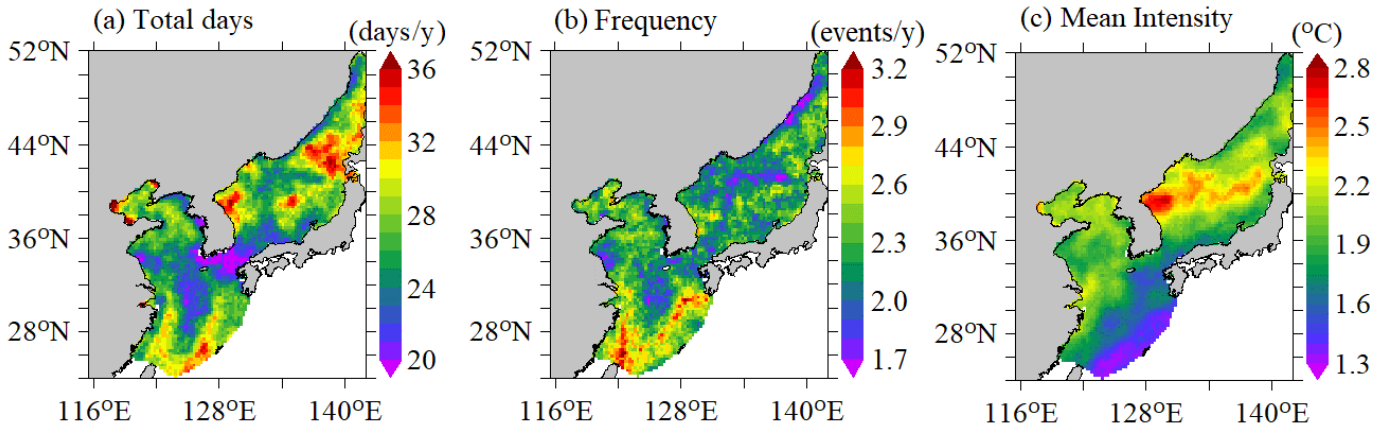

Figure 2. Spatial distribution of marine heatwave (MHW) characteristics averaged over 37 years (1982–2018) in the East Asian Marginal Seas. (**a**) Total days; (**b**) frequency; (**c**) mean intensity.

The spatial mean intensity of MHWs was 1.9 °C and ranged from 1.3 to 2.8 °C during the 37 years in the EAMS (Figure 2c). Regionally, the spatial mean was 2.1 °C in the EJS and 1.8 °C in the YECS; in particular, the subpolar front (SPF) of the EJS, around 40°N, experienced the greatest intensity at more than 2.6 °C.

Since the total days of MHWs were calculated as the multiplication of the duration and frequency, if the total days of MHWs were the same and the frequency was relatively small, the mean duration of the MHWs was rather long. Overall, MHWs in EJS, especially along the SPF, tended to be higher total days, lower frequency, and more intense, indicating that the relatively strong and long-lasting MHWs were mainly generated there rather than in YECS. In summary, the cumulative intensity of MHWs (i.e., sum of MHW intensity during MHW onset) in the EJS was stronger than in the YECS. These regional differences in MHW characteristics may have been induced by different MHW mechanisms.

3.2. Seasonal MHW Characteristics

To compare the seasonal characteristics of the MHWs in EAMS, we divided the MHW characteristics into four seasons: spring (April–June), summer (July–September), fall (October–December), and winter (January–March), based on the start date of the MHW (Figure 3).

Total days of MHWs in each season are compared in Figure 3a–d. In the EJS, the spatial mean of total MHW days was 5.6 days/year in spring, 9.7 days/year during summer, 6.3 days/year in the fall, and 5.9 days/year in winter. In the YECS, the spatial mean of total MHW days was 5.9 days/year in the spring, 8.6 days/year in summer, 6.0 days/year in the fall, and 5.6 days/year in winter. Regardless of the region, MHWs were approximately 65% more frequent in summer than in other seasons. The spatial distribution of the total MHW days had seasonal differences. A peak (reaching 10 days/year) was observed in the Bohai Bay in spring near the east coast of the Korean peninsula in the YS, along the west coast of Japan in summer, and along the SPF around 40°N in the fall and winter.

The frequency of MHWs (Figure 3e–h) was higher in summer than in other seasons, with a spatial mean of approximately 0.75 events/year in the EJS and 0.79 events/year in the YECS. The frequency of MHWs was 0.53, 0.45, and 0.44 events/year in the EJS, and 0.56, 0.50, and 0.50 events/year in the YECS, in the spring, fall, and winter, respectively. Thus, the numerous total MHW days in summer occurred because MHWs occurred 1.5 times more frequently than in other seasons.

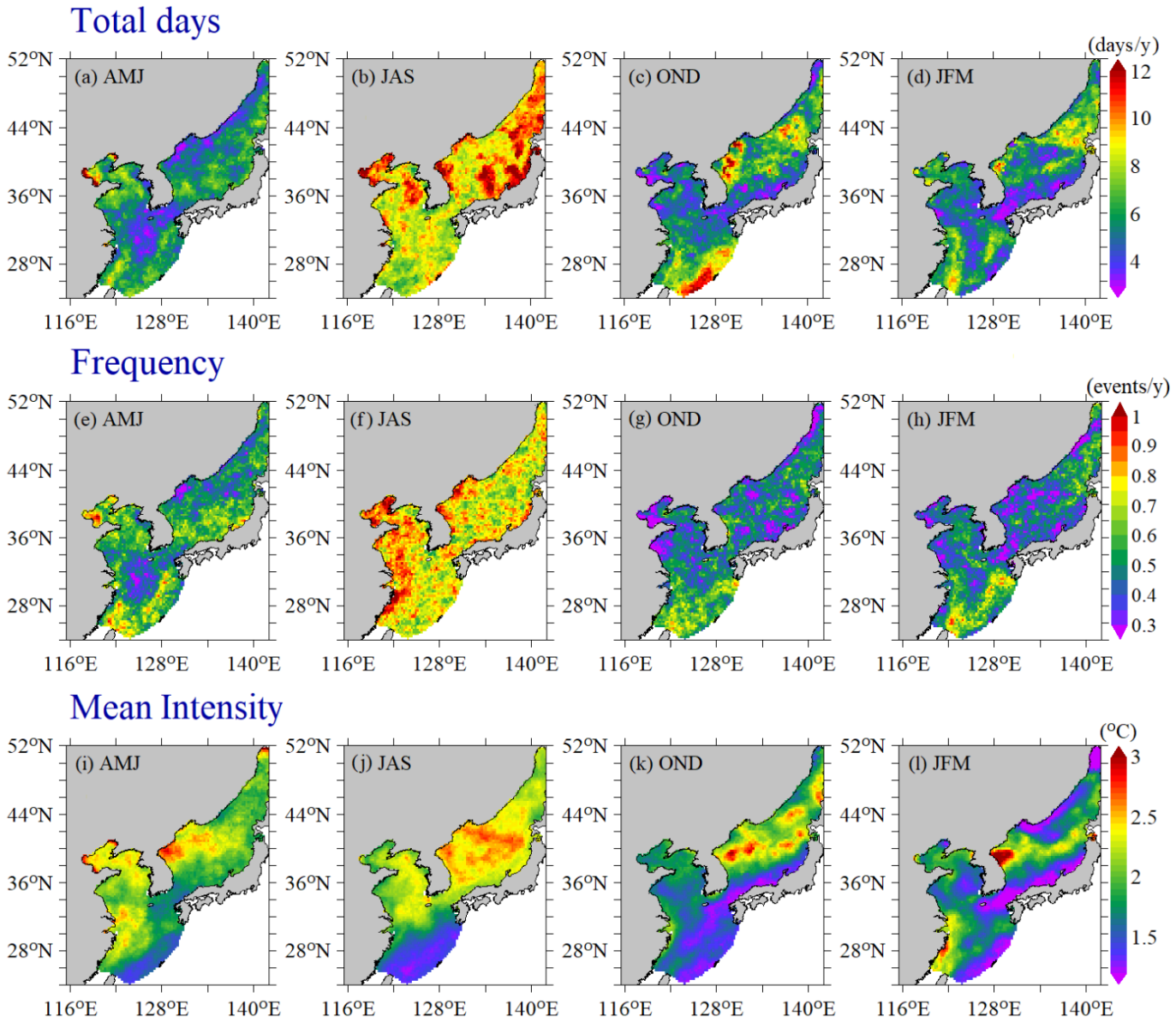

Figure 3. Spatial distribution of seasonal MHW characteristics for spring (April–June; AMJ), summer (July–September; JAS), fall (October–December; OND), and winter (January–March; JFM) from 1982 to 2020 in the EAMS. (**a**–**d**) Total days; (**e**–**h**) frequency; (**i**–**l**) mean intensity.

The spatial mean intensity of MHWs (Figure 3i–l) in the EJS was 2.1, 2.4, 2.0, and 1.7 °C in spring, summer, fall, and winter, respectively. In YECS, the intensity was 2.0, 1.9, 1.6, and 1.7 °C in spring, summer, fall, and winter, respectively. The spatial mean of the mean intensity of MHWs indicates the substantial differences (approximately 0.4 °C) between the EJS and YECS in summer and fall, unlike those in the spring and winter. Additionally, a strong mean intensity (greater than 2.5 °C) in each region appeared in different seasons. While the MHW intensity during summer (Figure 3j) can be characterized by the large-scale distribution of strong intensity over the EJS, the cold seasons (Figure 3k–l) showed a local frontal signature, revealing the zonal band of a large amplitude along the SPF around 40°N.

Overall, in spring, the total days of MHWs are less than those in other seasons. However, in the Bohai Sea, MHWs in spring tend to occur higher total days and be more frequent than in different regions and more intense than in other seasons. These intense and frequent MHWs in the Bohai Sea may be due to a relatively rapidly increasing SST trend [28].

The summer MHWs show more total days and are more frequent over a broad region in the EAMS, as well as the relatively expanded spatial distribution of strong intensity than in other seasons, indicating that the summer MHW is driven by large-scale forcing. On the other side, in the fall and winter, the total MHW days in the SPF were high (more than 10 days/year), but the frequencies were low (less than 0.4 events/year). In addition, the SPF mean intensity in this season is stronger than in other regions. The higher ratio regions of total days to frequency represented regions with longer MHW durations; thus, the SPF was the region for the occurrence of strong and long-lasting MHWs. As the spatial distribution differed seasonally, the mechanism of MHWs is expected to be seasonally different. In general, atmospheric influences are imposed over a wide area; these influences may induce MHWs mainly in spring and summer when strong MHWs appear over a wide region. Meanwhile, in the fall and winter, ocean processes seem to contribute to MHW generation, considering the strong mean intensity concentrated along the SPF formed by EKWC and NKCC.

To show the statistical variation of the seasonal MHW properties, a boxplot of the regional and seasonal MHW characteristics is presented (Figure 4). In summer, fall, and winter, the maximum and median total days of MHWs (Figure 4a) were higher in the EJS than in the YECS. The statistics in the YECS were slightly higher than those in the EJS in the spring. The differences in the maximum (median) total days of MHWs between the EJS and YECS were 8.8 (0.19) days/year in the spring, 1.1 (1.03) days/year in summer, 2.2 (0.57) days/year in the fall, and 2.5 (0.35) days/year in winter, with the most significant difference occurring in the spring (summer). The difference in the range of total days is the largest in spring, from 2 to 8.6 days/year in the EJS and from 2.1 to 17.4 days/year in the YECS.

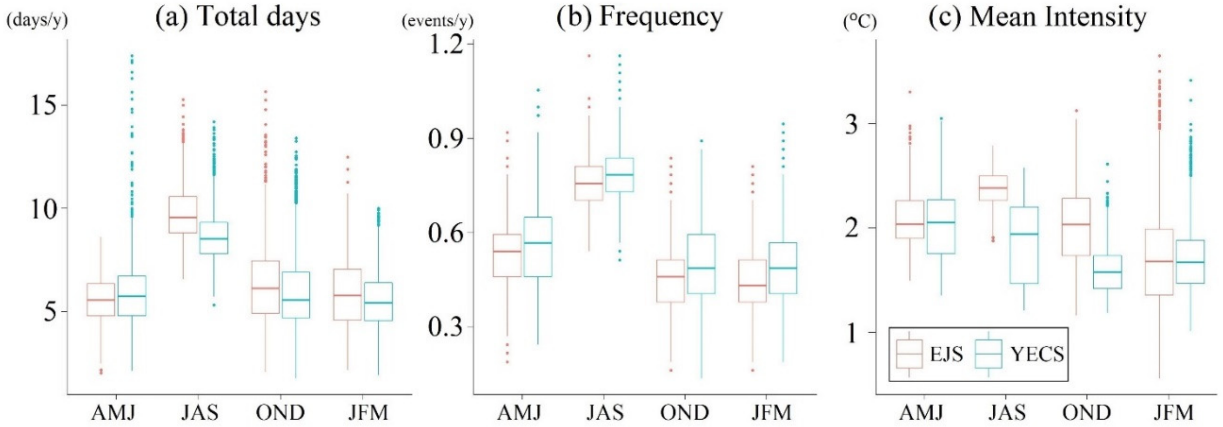

Figure 4. Boxplot of seasonal MHW characteristics in the EJS and YECS from 1982 to 2018: (**a**) Total days, (**b**) frequency, and (**c**) mean intensity. Horizontal lines inside the boxes indicate the median. The bottom and top of the box boundaries indicate the first and third quartiles, respectively.

The maximum MHW frequency was higher in the YECS than in the EJS, regardless of the season (Figure 4b). The regional difference between the EJS and the YECS was higher than 1.3 events/decade in winter and spring and lower than 0.5 events/decade in summer and fall, which was insignificant. The range difference in MHW frequency was insignificant by region.

The difference in the maximum of MHW mean intensity between the EJS and the YECS (Figure 4c) was weaker than 0.25 °C in spring, summer, and winter, but stronger than 0.5 °C in the fall. The median mean intensity in the EJS was the strongest during summer, but the range was from 1.88 to 2.79 °C, with a small deviation. The deviation was the greatest in winter, ranging from 0.56 to 3.65 °C. This is because the mean intensity of MHWs was concentrated at the SPF and weakly distributed in other regions. In general, regardless of the season, MHWs in the EJS tended to have a longer duration but were less

frequent, while in the YECS, the MHWs tended to have shorter durations while being more frequent.

To investigate the rate of MHWs with long durations, the average number of days per MHW occurrence (hereafter mean duration) was calculated using the median of total days and frequency (Figure 4a,b). In the EJS, the mean duration was 10.3 days/event in spring, 12.6 days/event in summer, 13.4 days/event in the fall, and 13.4 days/event in winter. In the YECS, the mean duration was 10.1 days/event in the spring, 10.9 days/event in summer, 11.4 days/event in the fall, and 11.2 days/event in winter. In fall and winter, the duration of MHWs in the EJS was more than 2 days longer than that in the YECS. These seasonal and regional MHW characteristics may be related to MHW mechanisms.

To relate the regional and seasonal MHW characteristics, the spatial proportion of seasons with the longest duration and the strongest mean intensity of MHWs for each grid in EAMS were investigated (Figure 5). The proportion of seasons with the longest MHW duration in the EJS was 3.6% in the spring, 42.7% in summer, 27.7% in the fall, and 26% in winter, and that in the YECS was 17.6% in the spring, 21.2% in summer, 39% in the fall, and 22.2% in winter. The longest MHW durations were typically observed in the fall and winter in the northern part of the EJS and in summer in the southern part of the EJS. In the YECS, the longest durations mainly occurred in the spring in the center, and in other seasons in the rest of the YECS. The strongest intensity of all events observed in the EJS was 23.6% in the spring, 55.9% in summer, 15.5% in the fall, and 5% in winter, and those in the YECS were observed as 36.1% in the spring, 38.3% in summer, 5.2% in the fall, and 20.4% in winter. Although MHWs with the strongest intensities occurred less frequently in the fall and winter in the EAMS (Figure 5d), in the SPF and the Kuroshio regions, they mainly occurred in fall and winter (Figure 5b), which is believed to be due to the influence of the ocean current. These regions also experienced the MHWs with the longest duration in the fall and winter (Figure 5a). Thus, in the fall and winter, the ocean currents likely contributed to the generation of the longest and strongest MHWs.

3.3. Mechanism of MHWs: Summer

To investigate the mechanism for the differences in MHW characteristics according to seasons and regions, changes in the atmosphere and ocean were investigated according to the occurrence of MHWs. The mechanism responsible for the occurrence of the MHW is expected to be distinct between summer and winter due to its different features: during summer, MHWs occur frequently, and regional differences in mean intensity are small. On the other hand, during winter, MHWs with strong intensity and long duration mainly occur along the SPF. The composite difference in atmospheric variables was calculated when the duration, mean intensity, and spatial coverage were all in the top third (hereafter strong MHW period) and the bottom third (hereafter weak MHW period).

During summer, the SST during strong MHW periods was higher over the EAMS than during weak MHW periods (Figure 6a). The total cloud cover was also low over the same region in the EAMS (Figure 6b). A smaller cloud fraction can induce strong MHWs by increasing the surface shortwave radiation, leading to a positive anomaly for ocean heating in the same region (Figure 6c). The wind speed at 10 m was weak, associated with the southerly wind anomalies during the strong MHW period. The weaker wind speeds increased the SST by reducing evaporation by decreasing the surface latent heat flux (Figure 6d,e). In addition, the southerly wind anomaly implies the advection of warm and moist air from the lower latitudes [37,38], which contributes to the induction of the MHWs. As a major cause of these changes, the 500 hPa geopotential height clearly shows a warm anomaly in Figure 6f, suggesting an intensified northwest flank of the subtropical high. In summary, the combined effect of atmospheric forcing under the expanding subtropical highs was closely related to the occurrence of MHWs in summer.

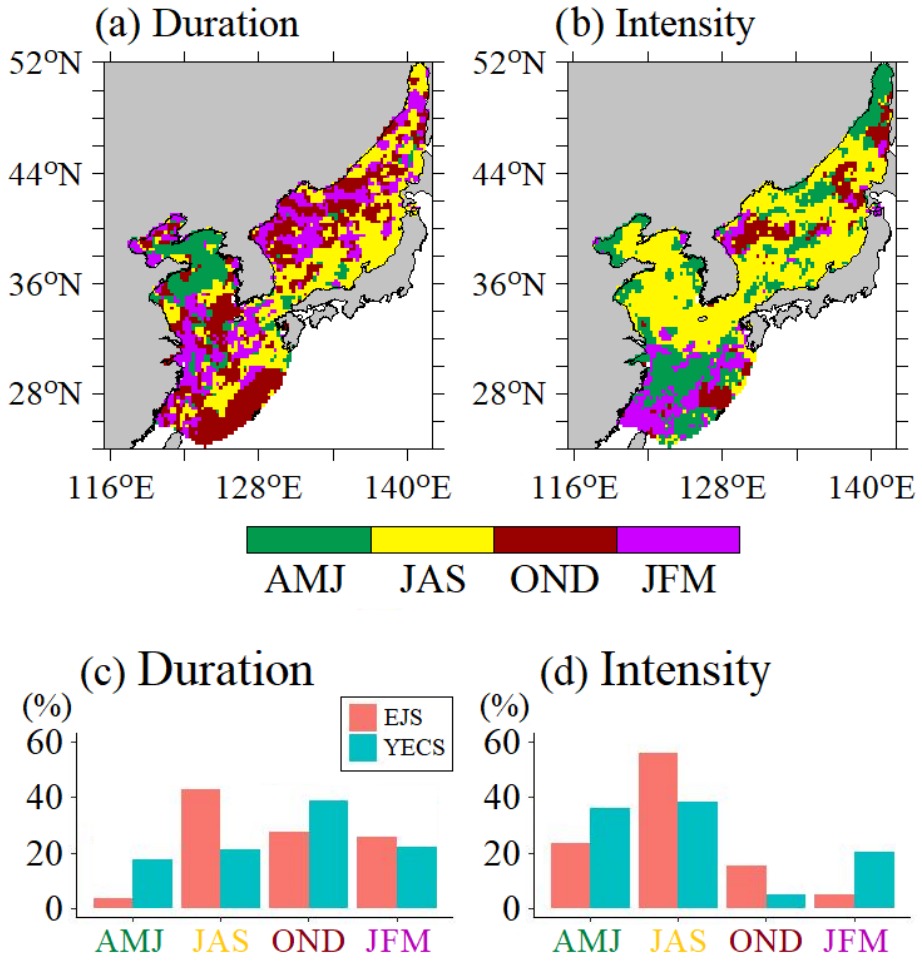

Figure 5. Spatial distribution (upper panels) and spatial ratio (bottom panels) of the season when MHWs have the longest duration (**a**,**c**) and strongest mean intensity (**b**,**d**).

3.4. Mechanism of MHWs: Winter

Regarding seasonal MHW characteristics, the strong mean intensity was characterized by large-scale distribution during summer, whereas in winter, strong mean intensity was concentrated along the SPF. In the SPF of the EJS, unlike the YECS, regional influences, such as ocean currents, are considered to be dominant. Thus, the mechanism of MHWs in winter was investigated by dividing the two regions (EJS and YECS), and a composite analysis was performed based on the characteristics of MHWs in each region (Figures 7 and 8).

In the YECS, the SST during the strong MHW period showed a higher positive anomaly than during the weak MHW period (Figure 7a). The total cloud cover decreased, which increased shortwave radiation (Figure 7b,c). The reduced wind speed at 10 m during the strong MHW period in the YECS led to the increase in SST, owing to a decrease in latent cooling through reduced evaporation and vertical ocean mixing (Figure 7d,e). The southeasterly wind anomaly shown in Figure 7d may have induced strong MHWs by reducing the cold air advection from the continent. The changes in 10 m wind and latent heat can be explained by a warm anomaly, as shown in Figure 7f, suggesting weaker continental highs. The warm anomaly also explains the reduced cloud formation as the cold air mass and its frontal system retreated northward (Figure 7b). In short, the general occurrence mechanism over the YECS during winter is similar to those over the EAMS during summer.

On the contrary, in the EJS, ocean dynamics, rather than atmospheric forcing, had a dominant effect on the occurrence of MHWs. When comparing the strong MHW period to the weak MHW period, the composite differences in total cloud cover and 10 m wind

were negligible and insignificant in most areas (not shown). Supporting this evidence, the shortwave radiation also decreased (Figure 8b), indicating that the atmospheric forcing had hardly contributed to the generation of MHWs. The intensified positive SST anomalies along the SPF (Figure 8a) corresponded to the enhanced latent heat flux (Figure 8c) into the atmosphere, which particularly coincided with where strong and long MHWs occurred. As atmospheric influences usually have a wide range of impacts, the enhanced heat transfer from the ocean to the atmosphere suggests the strong influence of the ocean on the atmosphere: the atmospheric variables respond to the oceanic-variables-derived MHW-related SST.

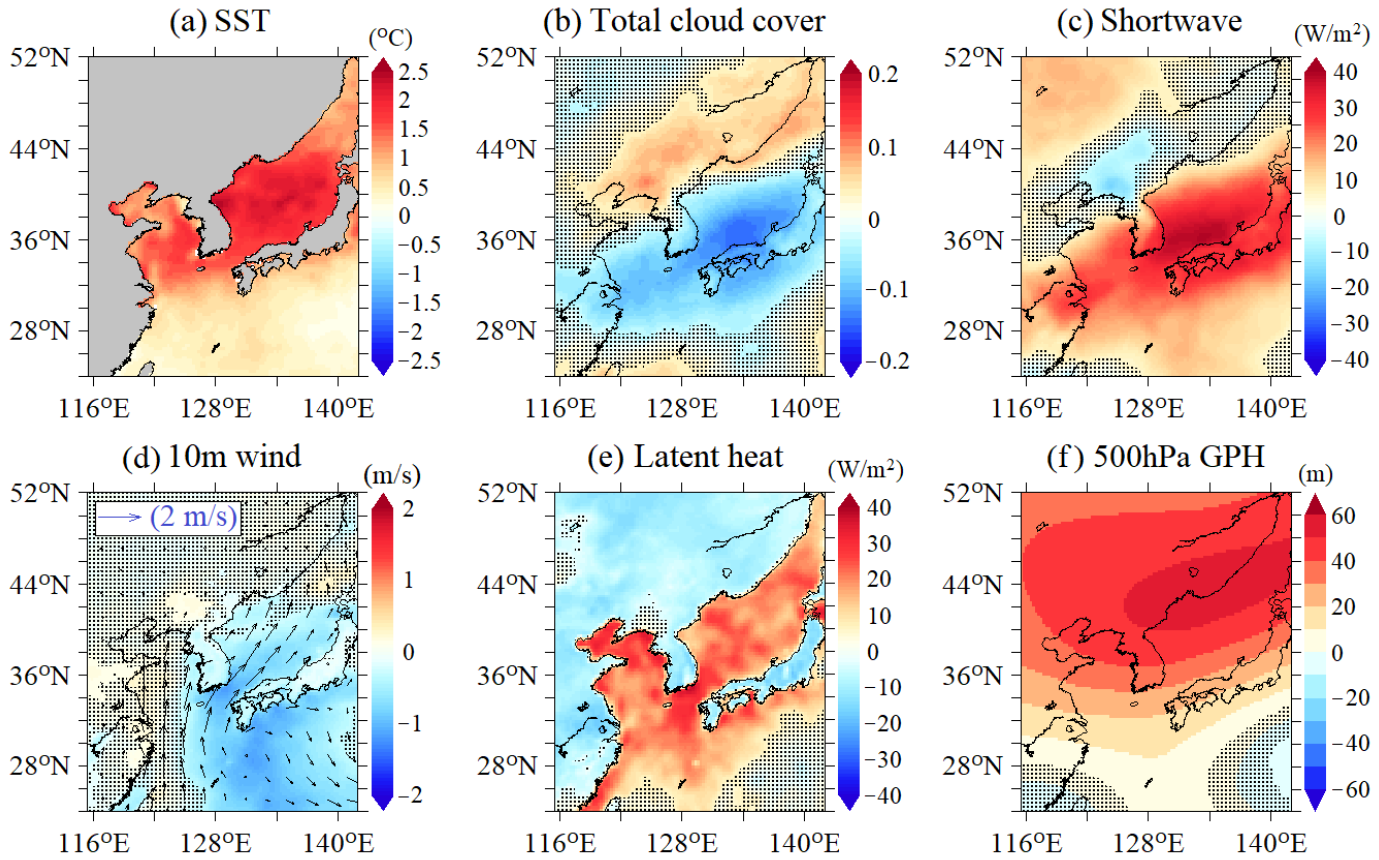

Figure 6. Composite differences during the top third (strong) and the bottom third (weak) MHW characteristics (duration, coverage, mean intensity) in summer (strong–weak). (**a**) Sea surface temperature, (**b**) total cloud cover, (**c**) shortwave radiation, (**d**) 10 m wind speed and direction, (**e**) latent heat flux (downward positive), and (**f**) 500 hPa geopotential height. The dotted areas indicate insignificant values at a 95% confidence level using Student *t*-test (*p*-value > 0.05).

The region where significantly stronger and longer MHWs occurred in winter coincides with the region where the SPF is generated between the EKWC and the NKCC. Therefore, to consider the influence of the ocean current on MHW occurrence, the composite differences in the surface ocean currents between the strong and weak MHW periods in the EJS were investigated using KHOA data (Figure 9). In a normal state, the EKWC flows northward along the east coast of Korea to the separation latitude of approximately 37–38°N [39] and flows eastward in meandering patterns along the SPF. In contrast, during the strong MHW period, the EKWC reaches 40°N (Figure 9a), and the ocean current flows eastward from approximately 39.5°N. This means that as the separation latitude and the SPF shift north, relatively warm water may flow toward higher latitudes, which may induce strong MHWs in winter. These northward shifts could be affected by the weakening of the cyclonic ocean circulations in the north EJS [40] via a decrease in the southward NKCC flows. The changes

in ocean circulation in the EJS were investigated through the composite differences in wind stress curl (Figure 9b). Although the changes in wind stress curl are insignificant at a 95% confidence level, the negative anomalies of the wind stress curl imply a northward shift of the EKWC. During the strong MHW period, the wind stress curl shows noticeable negative anomalies along the SPF to the Tsugaru Strait, where the edge of the cyclonic ocean circulation in the northern EJS is located [41]. These negative anomalies of the wind stress curl suggest a weakening of the cyclonic ocean circulation and thus NKCC weakening, which allows the EKWC to flow farther. In addition, the cyclonic circulation in the East Korean Bay (EKB) is also one of the major contributors to the separation of the EKWC from the coast [42,43]. The obvious negative anomalies of wind stress curl over the EKB may enhance a northward flowing of EKWC, compared with a weak MHW period in accordance with the development of the anticyclonic ocean circulation anomalies. In conclusion, the weakening of the two cyclonic ocean circulations may induce the northward shift of the SPF through the decrease in the NKCC. In addition to wind stress curl, surface heat flux may contribute to the northward shift of the SPF [44], which will be examined in detail in a future study on the northward shift of the SPF. In summary, atmospheric forcing plays a dominant role in MHW in the YECS, while ocean currents contribute greatly to MHW in the EJS in winter.

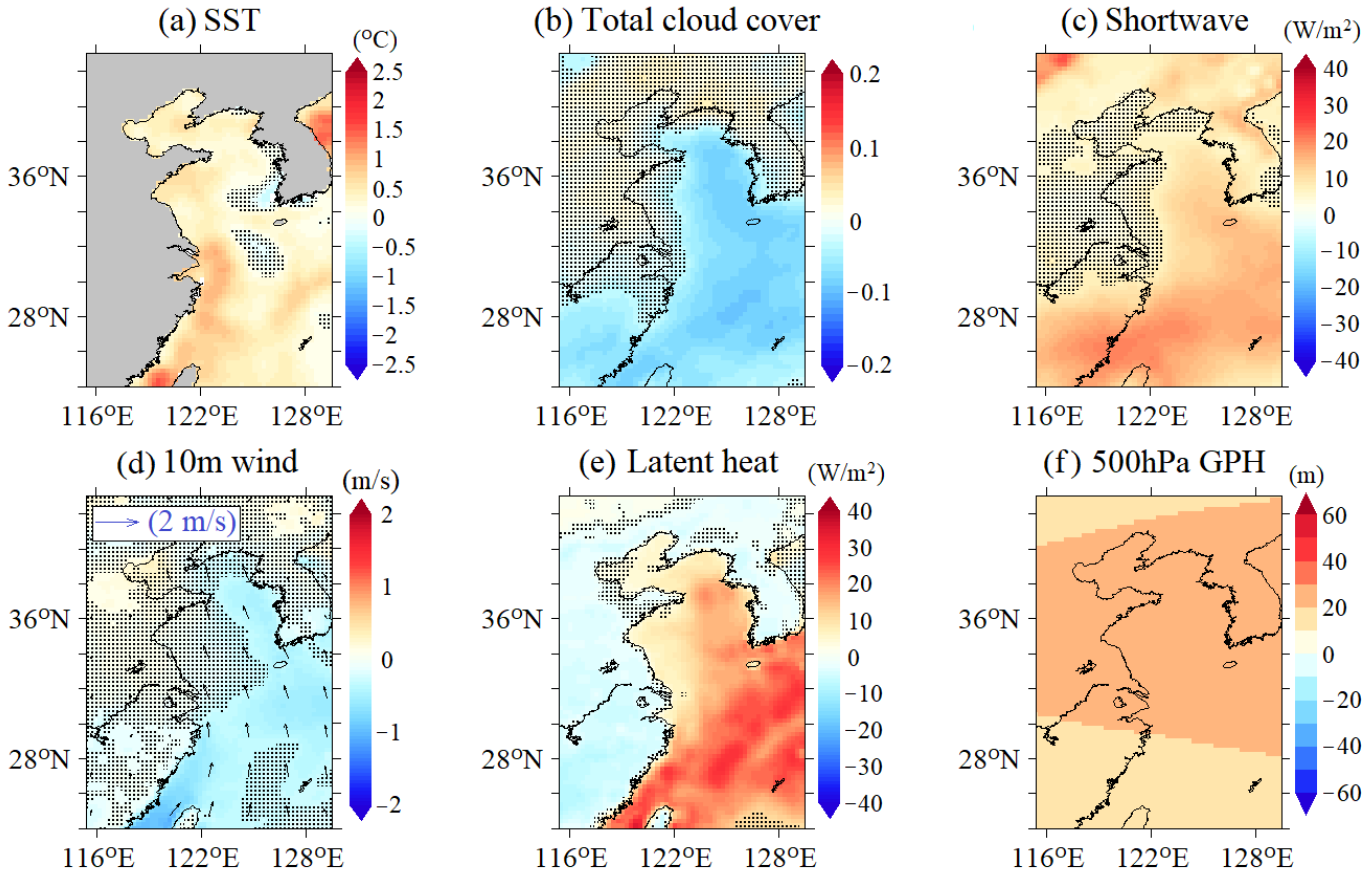

Figure 7. Composite differences during the top third (strong) and the bottom third (weak) MHW characteristics (duration, coverage, mean intensity) in YECS in winter (strong–weak). (**a**) Sea surface temperature, (**b**) total cloud cover, (**c**) shortwave radiation, (**d**) 10 m wind speed and direction, (**e**) latent heat flux (downward positive), and (**f**) 500 hPa geopotential height. The dotted areas indicate insignificant values at a 95% confidence level using Student *t*-test (*p*-value > 0.05).

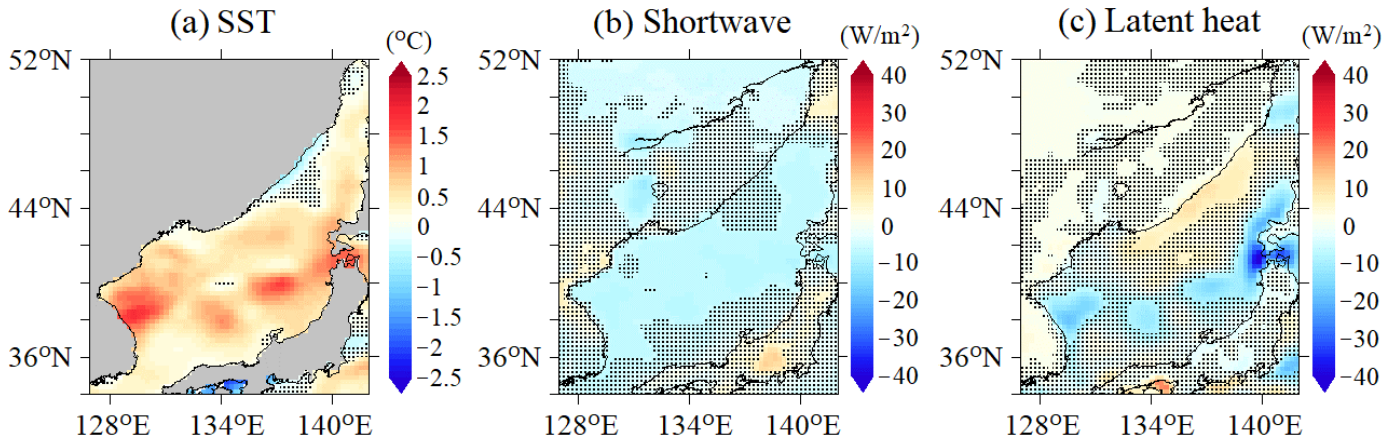

Figure 8. Composite difference during the top third (strong) and the bottom third (weak) MHW characteristics (duration, coverage, mean intensity) in EJS in winter (strong–weak). (**a**) Sea surface temperature, (**b**) shortwave radiation, and (**c**) latent heat flux (downward positive). The dotted areas indicate insignificant values at a 95% confidence level using Student *t*-test (*p*-value > 0.05).

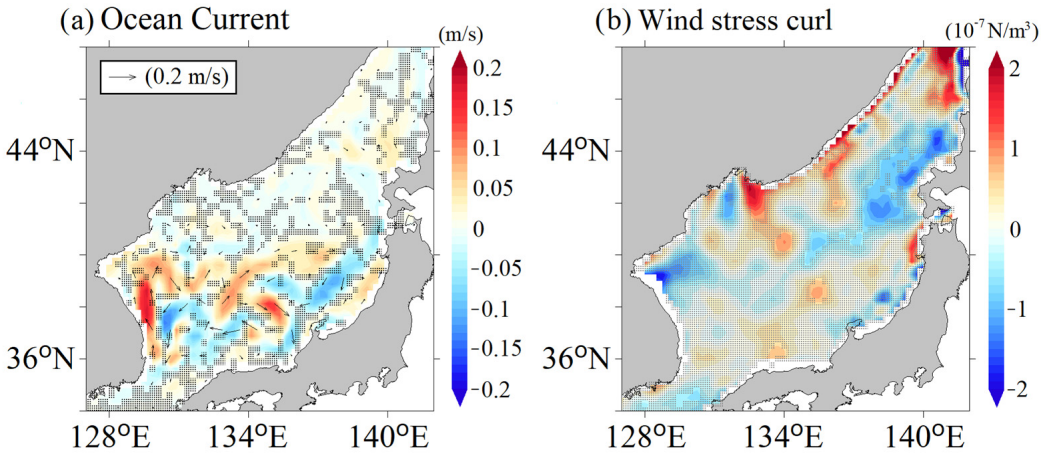

Figure 9. Composite difference of ocean currents and wind stress curl during the top third (strong) and the bottom third (weak) MHW characteristics (duration, coverage, mean intensity) in EJS in winter (strong–weak). The dotted areas indicate insignificant values at a 95% confidence level using Student *t*-test (*p*-value > 0.05).

4. Conclusions

In this study, we found that MHW mechanisms vary across seasons and regions in the EAMS, leading to seasonal and regional differences in the MHW characteristics. The summer MHWs occur mainly due to atmospheric forcing, including increased surface shortwave radiation and weakened wind over the western flanks of developing subtropical highs. In contrast, the winter MHW mechanisms differ by region. In the YECS, the MHWs are largely driven by atmospheric processes, while the MHWs in the EJS appear to be tied to oceanic heat transport or variability associated with a northward shift of the SPF, which may be due to weakened positive wind stress curl in the northern EJS. These ocean dynamics induce a spatial distribution of strong MHW along the SPF, whereas atmospheric forcing is attributed to a strong MHW over a wide region.

The MHW driving mechanisms across seasons and regions are primarily associated with regional SST warming dynamics. In the EAMS, the increasing mean SST mainly contributes to the increases in MHW total days from 1982 to 2017 [45]. During summer, the EJS SST increases by intensified solar radiation over the entire EJS, resulting in spatially homogeneous warming [46]. During winter, the southern EJS is mainly warmed by the Tsushima warm current [47–49]. The YECS, comprising continental shelf seas shallower

than 200 m depth, are mainly affected by seasonal variations in atmospheric forcing, such as wind and surface heat flux [50]. These previous studies support our conclusion that atmospheric forcing plays a dominant role in MHW occurrence in the YECS, whereas ocean currents contribute significantly to MHWs in the EJS in winter.

Although our study mainly investigated the local MHW mechanisms, we cannot exclude the fact that those mechanisms might be affected by natural variabilities, such as ENSO and PDO, through global-scale teleconnection. For instance, ENSO contributes to summer MHW occurrence via anomalous large-scale atmospheric circulations, where the anticyclonic circulation anomaly is enhanced over the western North Pacific as it changes from a warming to a cooling phase [11]. During the negative PDO phase, the transport of the Tsushima Warm Current tends to intensify heat supply to the EJS [51,52]. Clarifying how these natural variabilities contribute to the local MHW mechanisms in the EAMS would be an important topic for better understanding EAMS MHW occurrence, which should be further investigated.

More importantly, our results can contribute to an improved understanding of the physical drivers of regional MHWs, possibly resulting in enhanced seasonal predictability of MHWs in the EAMS. Furthermore, this seasonal predictability can contribute to the forecasting of atmospheric extremes as well as fluctuations in marine resources. For example, MHWs generated in the South Sea in summer can induce atmospheric heat waves on the Korean Peninsula [53]. Therefore, the significant regional and seasonal differences in the mechanism underlying MHW onset can provide a starting point for understanding the air–sea interaction between extreme climate events.

Author Contributions: Conceptualization, W.C. and C.J.J.; methodology, W.C.; software, W.C.; validation, M.B., Y.J., N.K. and Y.-G.H.; formal analysis, W.C.; data curation, W.C.; writing—original draft preparation, W.C. and C.J.J.; writing—review and editing, M.B., Y.J., N.K. and Y.-G.H.; visualization, W.C.; supervision, C.J.J.; funding acquisition, C.J.J. All authors have read and agreed to the published version of the manuscript.

Funding: This research was supported by the research programs of the Korea Institute of Ocean Science and Technology (PE99961).

Data Availability Statement: The SST data are available at https://www.ncei.noaa.gov/data/sea-surface-temperature-optimum-interpolation/v2.1/access/avhrr/, accessed on 31 March 2022. The ERA5 data are available at https://cds.climate.copernicus.eu/cdsapp#!/dataset/reanalysis-era5-single-levels?tab=form, accessed on 31 March 2022. The KHOA ocean current data were obtained from the Korea Hydrographic and Oceanographic Agency (http://www.khoa.go.kr/, (accessed on 24 December 2019)).

Acknowledgments: We sincerely thank Cheol-Ho Kim in KIOST for his comments on understanding the dynamics of the wind stress curl on the subpolar front shift. Furthermore, we would like to acknowledge YeonSoo Kim for designing Figure 1.

Conflicts of Interest: The authors declare no conflict of interest.

References

1. IPCC. Technical Summary. In *IPCC Special Report on the Ocean and Cryosphere in a Changing Climate*; Pörtner, H.-O., Roberts, D.C., Masson-Delmotte, V., Zhai, P., Poloczanska, E., Mintenbeck, K., Tignor, M., Alegría, A., Nicolai, M., Okem, A., et al., Eds.; Cambridge University Press: Cambridge, UK; New York, NY, USA, 2019.
2. Collins, M.; Sutherland, M.; Bouwer, L.; Cheong, S.M.; Frolicher, T.; DesCombes, H.J.; Roxy, M.K.; Losada, I.; McInnes, K.; Ratter, B.; et al. Extremes, Abrupt Changes and Managing Risk. 2019. Available online: http://ecite.utas.edu.au/148967/ (accessed on 10 December 2019).
3. Coumou, D.; Rahmstorf, S. A decade of weather extremes. *Nat. Clim. Change* **2012**, *2*, 491–496. [CrossRef]
4. Oliver, E.C.; Donat, M.G.; Burrows, M.T.; Moore, P.J.; Smale, D.A.; Alexander, L.V.; Benthuysen, J.A.; Feng, M.; Sen Gupta, A.; Hobday, A.J.; et al. Longer and more frequent marine heatwaves over the past century. *Nat. Commun.* **2018**, *9*, 1324. [CrossRef] [PubMed]
5. Ramírez, I.J.; Briones, F. Understanding the El Niño costero of 2017: The definition problem and challenges of climate forecasting and disaster responses. *Int. J. Disaster Risk Sci.* **2017**, *8*, 489–492. [CrossRef]
6. Alexander, D. *Natural Disasters*, 1st ed.; Routledge: London, UK, 2018.

7. Frölicher, T.L.; Fischer, E.M.; Gruber, N. Marine heatwaves under global warming. *Nature* **2018**, *560*, 360–364. [CrossRef]
8. Pearce, A.F.; Feng, M. The rise and fall of the "marine heat wave" off Western Australia during summer of 2010/2011. *J. Mar. Syst.* **2013**, *111*, 139–156. [CrossRef]
9. Wang, D.; Xu, T.; Fang, G.; Jiang, S.; Wang, G.; Wei, Z.; Wang, Y. Characteristics of Marine Heatwaves in the Japan/East Sea. *Remote Sens.* **2022**, *14*, 936. [CrossRef]
10. Joh, Y.; Di Lorenzo, E. Increasing coupling between NPGO and PDO leads to prolonged marine heatwaves in the Northeast Pacific. *Geophys. Res. Lett.* **2017**, *44*, 11–663. [CrossRef]
11. Lee, S.; Park, M.S.; Kwon, M.; Kim, Y.H.; Park, Y.G. Two major modes of East Asian marine heatwaves. *Environ. Res. Lett.* **2020**, *15*, 074008. [CrossRef]
12. Oliver, E.C.; Lago, V.; Hobday, A.J.; Holbrook, N.J.; Ling, S.D.; Mundy, C.N. Marine heatwaves off eastern Tasmania: Trends, interannual variability, and predictability. *Prog. Oceanogr.* **2018**, *161*, 116–130. [CrossRef]
13. Di Lorenzo, E.; Mantua, N. Multi-year persistence of the 2014/15 North Pacific marine heatwave. *Nat. Clim. Change* **2016**, *6*, 1042–1047. [CrossRef]
14. Bates, B.; Kundzewicz, Z.; Wu, S.; Palutikof, J.P. *Climate Change and Water*; Technical Paper of the IPCC; IPCC Secretariat: Geneva, Switzerland, 2008.
15. Hayashida, H.; Matear, R.J.; Strutton, P.G. Background nutrient concentration determines phytoplankton bloom response to marine heatwaves. *Glob. Change Biol.* **2020**, *26*, 4800–4811. [CrossRef] [PubMed]
16. Lim, Y.K.; Park, B.S.; Kim, J.H.; Baek, S.S.; Baek, S.H. Effect of marine heatwaves on bloom formation of the harmful dinoflagellate *Cochlodinium polykrikoides*: Two sides of the same coin? *Harmful Algae* **2021**, *104*, 102029. [CrossRef] [PubMed]
17. Garrabou, J.; Coma, R.; Bensoussan, N.; Bally, M.; Chevaldonné, P.; Cigliano, M.; Díaz, D.; Harmelin, J.G.; Gambi, M.C.; Kersting, D.K.; et al. Mass mortality in Northwestern Mediterranean rocky benthic communities: Effects of the 2003 heat wave. *Glob. Change Biol.* **2009**, *15*, 1090–1103. [CrossRef]
18. Feng, M.; McPhaden, M.J.; Xie, S.P.; Hafner, J. La Niña forces unprecedented Leeuwin Current warming in 2011. *Sci. Rep.* **2013**, *3*, 1277. [CrossRef]
19. Benthuysen, J.; Feng, M.; Zhong, L. Spatial patterns of warming off Western Australia during the 2011 Ningaloo Niño: Quantifying impacts of remote and local forcing. *Cont. Shelf Res.* **2014**, *91*, 232–246. [CrossRef]
20. Wernberg, T.; Smale, D.A.; Tuya, F.; Thomsen, M.S.; Langlois, T.J.; De Bettignies, T.; Bennett, S.; Rousseaux, C.S. An extreme climatic event alters marine ecosystem structure in a global biodiversity hotspot. *Nat. Clim. Change* **2012**, *3*, 78–82. [CrossRef]
21. Smale, D.A.; Wernberg, T. Extreme climatic event drives range contraction of a habitat-forming species. *Proc. R. Soc. B Biol. Sci.* **2013**, *280*, 20122829. [CrossRef]
22. Mills, K.E.; Pershing, A.J.; Brown, C.J.; Chen, Y.; Chiang, F.-S.; Holland, D.S.; Lehuta, S.; Nye, J.A.; Sun, J.C.; Thomas, A.C.; et al. Fisheries management in a changing climate: Lessons from the 2012 ocean heat wave in the Northwest Atlantic. *Oceanography* **2013**, *26*, 191–195. [CrossRef]
23. Kain, J.M. The seasons in the subtidal. *Brit. Phycol. J.* **1989**, *24*, 203–215. [CrossRef]
24. Atkinson, J.; King, N.G.; Wilmes, S.B.; Moore, P.J. Summer and winter marine heatwaves favor an invasive over native seaweeds. *J. Phycol.* **2020**, *56*, 1591–1600. [CrossRef]
25. Santelices, B. Patterns of reproduction, dispersal and recruitment in seaweeds. *Oceanogr. Mar. Biol. Annu. Rev.* **1990**, *28*, 177–276.
26. Lotze, H.K.; Worm, B.; Sommer, U. Strong bottom-up and top-down control of early life stages of macroalgae. *Limnol. Oceanogr.* **2001**, *46*, 749–757. [CrossRef]
27. Yao, Y.; Wang, J.; Yin, J.; Zou, X. Marine heatwaves in China's marginal seas and adjacent offshore waters: Past, present, and future. *J. Geophys. Res. Ocean.* **2020**, *125*, e2019JC015801. [CrossRef]
28. Park, S.; Chu, P.C. Interannual SST variability in the Japan/East Sea and relationship with environmental variables. *J. Oceanogr.* **2006**, *62*, 115–132. [CrossRef]
29. Yeh, S.W.; Park, Y.G.; Min, H.; Kim, C.H.; Lee, J.H. Analysis of characteristics in the sea surface temperature variability in the East/Japan Sea. *Prog. Oceanogr.* **2010**, *85*, 213–223. [CrossRef]
30. Park, T.; Jang, C.J.; Jungclaus, J.H.; Haak, H.; Park, W. Effects of the Changjiang river discharge on sea surface warming in the Yellow and East China Seas in summer. *Cont. Shelf Res.* **2011**, *31*, 15–22. [CrossRef]
31. Park, K.A.; Lee, E.Y.; Chang, E.; Hong, S. Spatial and temporal variability of sea surface temperature and warming trends in the Yellow Sea. *J. Mar. Syst.* **2015**, *143*, 24–38. [CrossRef]
32. Reynolds, R.W.; Rayner, N.A.; Smith, T.M.; Stokes, D.C.; Wang, W. An improved in situ and satellite SST analysis for climate. *J. Clim.* **2002**, *15*, 1609–1625. [CrossRef]
33. Hersbach, H.; Dee, D. ERA5 reanalysis is in production. In *ECMWF Newsletter*; European Centre for Medium-Range Weather Forecasts: Reading, UK, 2016; Volume 147.
34. Choi, B.J.; Byun, D.S.; Lee, K.H. Satellite-altimeter-derived East Sea surface currents: Estimation, description and variability pattern. *Sea* **2012**, *17*, 225–242. [CrossRef]
35. Hobday, A.J.; Alexander, L.V.; Perkins, S.E.; Smale, D.A.; Straub, S.C.; Oliver, E.C.; Benthuysen, J.A.; Burrows, M.T.; Donat, M.G.; Feng, M.; et al. A hierarchical approach to defining marine heatwaves. *Prog. Oceanogr.* **2016**, *141*, 227–238. [CrossRef]
36. Schlegel, R.W.; Smit, A.J. HeatwaveR: A central algorithm for the detection of heatwaves and cold-spells. *J. Open Source Softw.* **2018**, *3*, 821. [CrossRef]

37. Ham, Y.-G.; Chikamoto, Y.; Kug, J.-S.; Kimoto, M.; Mochizuki, T. Tropical Atlantic–Korea teleconnection pattern during boreal summer season. *Clim. Dyn.* **2017**, *49*, 2649–2664. [CrossRef]
38. Ham, Y.-G.; Kug, J.-S.; Kang, I.-S. Role of moist energy advection in formulating anomalous Walker Circulation associated with ENSO. *J. Geophy. Res.* **2007**, *112*, D24105. [CrossRef]
39. Park, K.; Park, J.E.; Choi, B.J.; Byun, D.S.; Lee, E.I. An oceanic current map of the East Sea for science textbooks based on scientific knowledge acquired from oceanic measurements. *Sea J. Korean Soc. Oceanogr.* **2013**, *18*, 234–265.
40. Kim, C.H.; Yoon, J.H. Modeling of the wind-driven circulation in the Japan Sea using a reduced gravity model. *J. Oceanogr.* **1996**, *52*, 359–373. [CrossRef]
41. Yarichin, V.G. Steady state of the Japan Sea circulation. *Probl. Oceanogr.* **1980**, 46–61.
42. Yoon, J.H.; Abe, K.; Ogata, T.; Wakamatsu, Y. The effects of wind-stress curl on the Japan/East Sea circulation. *Deep. Sea Res. Part II Top. Stud. Oceanogr.* **2005**, *52*, 1827–1844. [CrossRef]
43. Park, Y.; Shin, H.R.; Yoon, J.H.; Kim, C.H.; Yoshikawa, Y. Simulation of eddy-driven deep circulation in the East/Japan Sea by using a three-layer model with wind, throughflow and deep water formation forcings. *J. Mar. Syst.* **2015**, *150*, 41–55. [CrossRef]
44. Kim, D.; Shin, H.R.; Kim, C.H.; Hirose, N. Characteristics of the East Sea (Japan Sea) circulation depending on surface heat flux and its effect on branching of the Tsushima Warm Current. *Cont. Shelf Res.* **2020**, *192*, 104025. [CrossRef]
45. Oliver, E.C. Mean warming not variability drives marine heatwave trends. *Clim. Dyn.* **2019**, *53*, 1653–1659. [CrossRef]
46. Park, K.A. Spatial and Temporal Variability of Sea Surface Temperature and Sea Level Anomaly in the East Sea Using Satellite Data (NOAA/AVHRR, TOPEX/ALT). Ph.D. Dissertation, Seoul National University, Seoul, Korea, 1996; p. 294.
47. Chu, P.C.; Lan, J.; Fan, C.W. Japan Sea circulation and thermohaline structure, Part 1, Climatology. *J. Phys. Oceanogr.* **2001**, *31*, 244–271. [CrossRef]
48. Chu, P.C.; Lan, J.; Fan, C.W. Japan Sea circulation and thermohaline structure, Part 2, A variational P-vector method. *J. Phys. Oceanogr.* **2001**, *31*, 2886–2902. [CrossRef]
49. Chu, P.C.; Wang, G.H.; Chen, Y.C. Japan Sea circulation and thermohaline structure, Part 3, Autocorrelation functions. *J. Phys. Oceanogr.* **2002**, *32*, 3596–3615. [CrossRef]
50. Chu, P.C.; Fralick, C.R., Jr.; Haeger, S.D.; Carron, M.J. A parametric model for the Yellow Sea thermal variability. *J. Geophys. Res. Ocean.* **1997**, *102*, 10499–10507. [CrossRef]
51. Gordon, A.L.; Giulivi, C.F. Pacific decadal oscillation and sea level in the Japan/East Sea. *Deep. Sea Res. I* **2004**, *51*, 653–663. [CrossRef]
52. Andres, M.; Park, J.; Mark, W.; Zhu, X.; Nakamura, H.; Kim, K.; Chang, K. Manifestation of the Pacific Decadal Oscillation in the Kuroshio. *Geophys. Res. Lett.* **2009**, *36*, L16602. [CrossRef]
53. Ham, Y.G.; Na, H.Y. Marginal sea surface temperature variation as a pre-cursor of heat waves over the Korean Peninsula. *Asia-Pac. J. Atmos. Sci.* **2017**, *53*, 445–455. [CrossRef]